Measurement of Low Plasma Densities in a Magnetic Field

FRANCIS F. CHEN, CLAUDE ETIEVANT,* AND DAVID MOSHER
Plasma Physics Laboratory, Princeton University, Princeton, New Jersey
(Received 19 September 1967)

Absolute measurements of plasma density in the range 8×10^8 to 3×10^{11} cm^{-3} were made in a potassium plasma by four methods: (1) Langmuir probes, (2) microwave cavity, (3) microwave interferometry, and (4) propagation of electrostatic waves. Agreement to $\approx 25\%$ between the probe and microwave measurements was achieved by careful application of probe theory. By contrast, indiscriminate use of probe theory would lead to an error of 600% at low densities. The fourth method, though less accurate, was found to be a useful independent check.

I. INTRODUCTION

Recently there has been much experimental interest in plasmas in the density range $n = 10^8$ to 10^{11} cm^{-3} because of the relatively stable plasmas possible at these low densities in alkali-metal plasmas, in multipoles, and in stellarators. The problem of measuring the absolute plasma density accurately is, however, not trivial. The Langmuir probe, an old standby because it is easy to use, gives results which are not easy to interpret when the ratio $\xi_p \equiv r_p/\lambda_D$ is not much larger than unity and when there is a strong magnetic field. Here r_p is the probe radius and λ_D the Debye length of the repelled species. In the region $\xi_p \approx 1$, the probe current is not proportional to n, and even relative densities measured by probes may be in error. The primary aim of this experiment is to show that meticulous use of probe theory and proper design of probes can lead to trustworthy determinations of absolute density. This is described in Sec. II. As an independent measure of density, we have used the shift in resonance of a microwave cavity; this is described in Sec. III. At densities greater than 10^{10} cm^{-3}, the latter method fails. We then used microwave interferometry, as described in Sec. IV. Interferometry in turn fails at low densities; in our experiment the two types of measurements unfortunately did not overlap.

We also tested a new method employing the propagation of longitudinal plasma waves between two probes. This method is a useful independent check on Langmuir probes because it does not require additional equipment in the vacuum chamber and is not susceptible to changes in probe collection area or surface conditions. In principle, the theory should be simpler than for the closely related method of resonance probes; however, the results shown in Sec. V show that this may not be the case. The various methods are compared in Sec. VI.

Probe theory is particularly simple when ξ_p is large ($\gg 10$) and the sheath thin, so that the collection area is essentially the geometrical area of the probe; or when ξ_p is small ($\ll 1$) and the sheath very thick, so that the probe current is governed by orbital motion, and the potential distribution around the probe need not be computed.[1] When there is a strong magnetic field, one is forced to make ξ_p small for the following reason. It is clear that in a nearly collisionless plasma, if the ion Larmor radius r_L is much less than r_p, the probe will quickly drain the plasma from the lines of force intercepting the probe, and the plasma density will be greatly perturbed. The probe current then no longer depends so much on local density as on the mechanisms of plasma production and diffusion. (It is, of course, out of the question to use electron collection except in extremely low magnetic fields.) To avoid perturbing the plasma, one must make $r_p \ll r_L$, or, more accurately, $r_s \ll r_L$, where r_s is the "absorption radius" defining the effective collecting area. Note that this condition applies not only to the probe tip but also to any part of the insulator or support structure that is immersed in the plasma. For the densities we are considering, it is generally not possible to satisfy $\xi_p \gg 10$ and $r_p \ll r_L$ at the same time.

On the other hand, the lower limit to r_p is set only by the physical strength of the probe and by the minimum probe current necessary to obtain the required frequency response. For cylindrical probes, the computations of Laframboise[2] show that the orbital-motion theory of Langmuir is ac-

* On leave from Centre d'Études Nucléaires, Fontenay-aux-Roses (Seine), France.

[1] F. F. Chen, in *Plasma Diagnostic Techniques*, R. H. Huddlestone and S. L. Leonard, Eds. (Academic Press Inc., New York, 1965), Chap. 4.

[2] J. G. Laframboise, University of Toronto, Institute for Aerospace Studies Report 100 (1966).

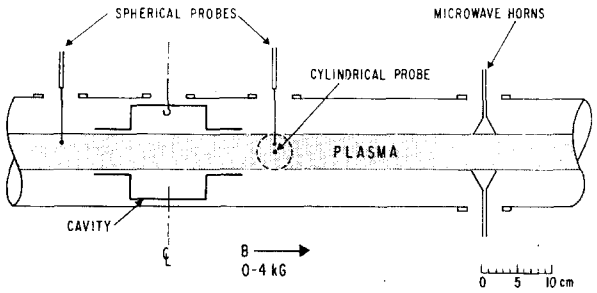

FIG. 1. Scale drawing of the placement of diagnostic equipment near the midplane of the plasma. The probes could be moved radially by remote control or swung manually about an external pivot to sample an entire cross section of the plasma.

curate for $\xi_p < 5$, and this is easy to satisfy. Frequency response can always be improved at the expense of spatial resolution by making the probe longer. Nonetheless, many experiments in the past have been done with cylindrical probes such that $\xi_p \gtrsim 5$; as will be shown in Sec. II, such probes do not give an accurate measurement of density unless the accurate theoretical results of Lam[3] or Laframboise[2] are used.

The main disadvantage of cylindrical probes is that the potential falls off slowly with radius, so that r_s can be much larger than λ_D. At low densities the length l of the probe must then be much greater than r_s, and hence extremely large compared to r_p, in order to avoid end-effects. In other words, only a very long probe will accurately approximate the infinite cylinder that the theory requires. For this and other reasons enumerated previously,[4] we consider spherical probes to be more reliable for absolute density measurements. Unfortunately, the simple orbital-motion theory is almost never valid for spheres for two reasons. First, the need for a support wire much smaller in diameter than the sphere makes $\xi_p \leq 1$ difficult to achieve; second, the orbital-motion approximation is useful for spheres only for $\xi_p \ll 1$, as shown clearly by the curves of Laframboise.[2] In the range $1 < \xi_p < 100$, which one usually has to contend with when using spherical probes, it is necessary to use either the boundary-layer method of Lam,[3] which assumes a monoenergetic distribution function, or the recent exact numerical computations of Laframboise[2] for a Maxwellian distribution function.

The present experiment was carried out in a thermally ionized potassium plasma 5.1 cm in diameter and 326 cm long. The temperature was

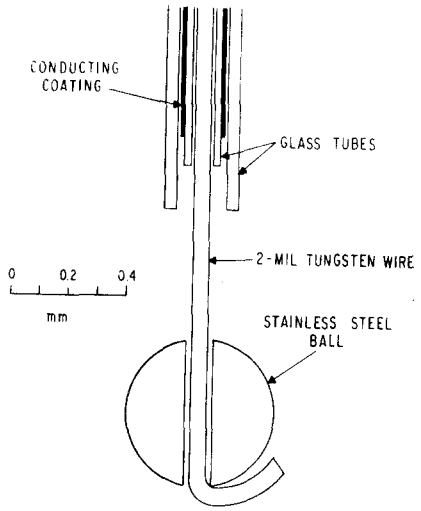

FIG. 2. Scale drawing of a spherical probe tip.

$kT_e = 0.22$ eV; and we assumed $T_i = T_e$, as is normal in this type of plasma. Since the base pressure was below 5×10^{-6} Torr and the neutral K pressure was kept below 10^{-8} Torr by water-cooled walls and liquid N_2 "cold-fingers," the plasma was essentially collisionless. The plasma density was varied by controlling the flux of neutral potassium impinging on the hot tungsten plates at both ends of the column. The fluxes from the two ends were kept balanced so that there was no unidirectional drift of plasma at the midplane. The experiment was carried out in a small section of the plasma near the midplane, as shown in Fig. 1. Further details on the apparatus may be found elsewhere.[5] Note that in this experiment solid end plates were used, rather than the ones with a central hole used for shear stabilization experiments in the same device.

II. LANGMUIR PROBES

A. Construction

Figure 2 is a scale drawing of the probe tip. The probes were coaxially shielded, the outside diameter of the outer capillary tube being 0.3 mm. This is approximately 0.15 Larmor diameters at the maximum field of 4 kG. To make a cylindrical probe, the 50-μ-diam central tungsten lead was simply cut off at a length of approximately 2 mm, so that $l/r_p \approx 80$. Spherical probes were made by threading the central lead through a 100-μ-diam hole in a 0.5-mm-diam stainless steel ball machined on a lathe. The wire was then bent and cut. A spotweld was usually not necessary for electrical contact.

[3] S. H. Lam, Phys. Fluids **8**, 1002 (1965).
[4] F. F. Chen, J. Nucl. Energy Pt. **C7**, 47 (1965).
[5] F. F. Chen, in *Proceedings of the Conference on Physics of Quiescent Plasmas* (Laboratori Gas Ionizzati, Frascati, Italy, 1967), Pt. I, p. 145.

B. Contamination

In a cesium or potassium plasma the surface condition of a probe is rather delicate, and it is necessary to monitor the probe characteristic every few minutes to be sure that the surface is not contaminated. Normally, one tries to keep the probe tip covered with potassium, which has a work function about 2.8 V lower than for tungsten. At low plasma densities, however, this layer of potassium is rather thin and is likely to come off when electrons are collected. The change in work function manifests itself as a hysteresis effect in the probe characteristic. Ion currents are not greatly affected by this. In addition, a layer of poorly conducting material often forms on the probe surface. This manifests itself in a decrease in the slope of the transition region of the probe characteristic, indicating a spuriously high electron temperature. To eliminate this layer, we found it necessary to outgas the probes periodically by applying a large positive potential (50–500 V, depending on the density). Cylindrical probes were more easily outgassed than spherical probes because the latter could not be heated to redness before the support wire became too hot. Again, this effect had comparatively little influence on saturation ion current.

However, if an insulating layer covered *part* of the probe surface, so that the collecting area was decreased, the ion saturation curve could not be fitted to theory. An example is shown in Fig. 3, where it is seen that if one fits the absolute magnitude of the ion current J_i to a theoretical curve using the full probe area, then the slope would not fit. Such a comparison is in fact a good check on probe contamination. In earlier work we often observed cylindrical-probe curves varying not as $-V_p^{\frac{1}{2}}$, as they should, but more nearly as $-V_p$, as if a spherical probe were being used. We attributed this to collection from the end of the cylinder and therefore resorted to using spherical probes; but it is now clear that at least part of the discrepancy was due to contamination.

C. Measurement of T_e

Since electrons are emitted thermionically from the end plates and the sheaths there are kept electron-rich so that electrons can communicate freely with the end plates, the electron temperature T_e should be very nearly equal to the end-plate temperature T_c. Figure 4 shows a direct measurement of T_e from the probe characteristic; agreement with T_e is within experimental error. However, agreement is not always this good. We have observed

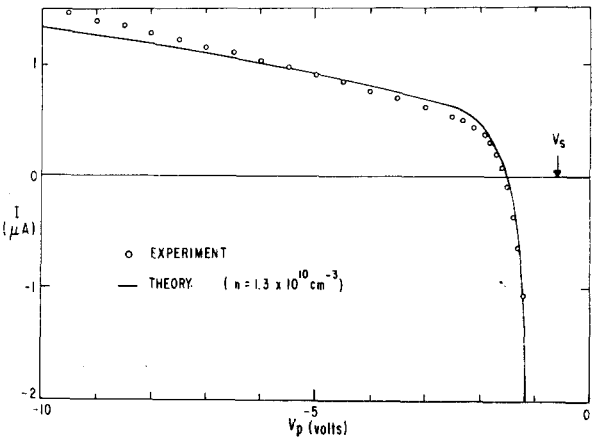

FIG. 3. Example of a cylindrical-probe characteristic (current I versus probe potential V_p) in the saturation ion current region when the probe is contaminated. Both the slope and the magnitude of J_i cannot be fitted to theory simultaneously.

electron temperatures as much as 30% higher than T_c; but we do not know whether T_e was actually higher, whether the probe was contaminated in such a way as to preserve the straight-line fit, or whether there is an unexpected effect from oscillations or the magnetic field. We have assumed $T_e = T_c$; if T_e is really greater than T_c, our data would fit theory better.

In Fig. 4, I_e was derived from the total probe current J by subtracting the ion current obtained by straight-line extrapolation (the dashed line in Figs. 5 and 6). In principle, I_i can be computed

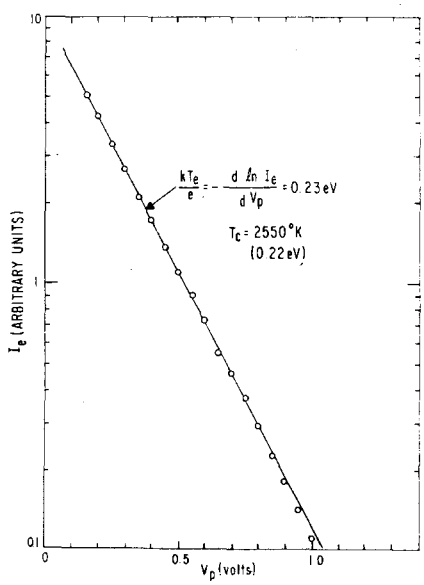

FIG. 4. Determination of electron temperature from the semilogarithmic plot of electron current I_e versus V_p. In this case, T_e agreed well with the end plate temperature T_c, as measured by optical pyrometer.

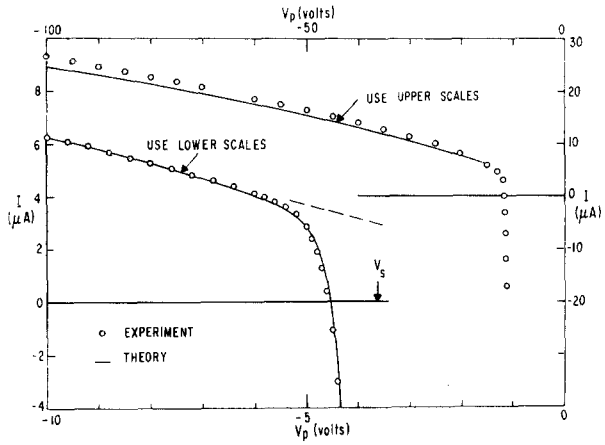

FIG. 5. Comparison of measured and computed I–V curves for a spherical probe. The agreement is absolute; there were no adjustable parameters. The theoretical curve is based on the density (2.05×10^{10} cm^{-3}) measured by the microwave cavity, and a 20% correction was made for the current collected on the unshielded lead. The position of the space potential V_s was computed, not adjusted. Laframboise's theory was used for $\eta_p \leq 25$, and the modified Lam theory was used for $\eta_p > 25$.

from theory, with the use of the measured value of T_e, and a more accurate subtraction of I_i made to obtain a better straight line for T_e. In practice, such an iteration procedure gave a negligible improvement in view of the 10% accuracy of the experiment.

D. Probe Theory

Since we attempt to work with $r_p \ll r_L$, we can use existing theories on ion collection in a collisionless plasma without a magnetic field. In the limit

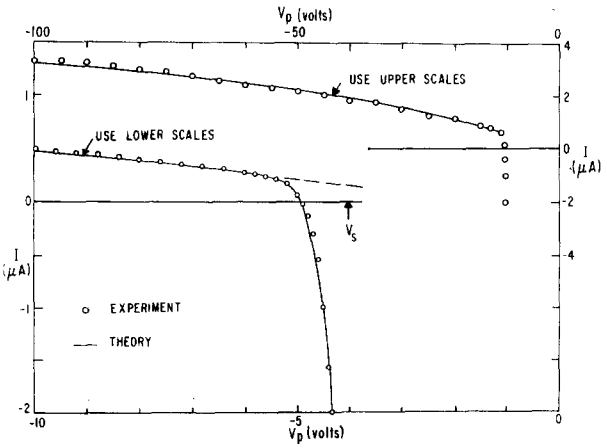

FIG. 6. Comparison of measured and computed I–V curves for a cylindrical probe. Here the assumed density (5.7×10^9 cm^{-3}) was adjusted for a fit at one point; V_s was not adjusted. Laframboise's theory was used for $\eta_p \leq 25$; Langmuir's orbital-motion theory was used for $\eta_p > 25$.

$\xi_p \ll 1$, the probe current for a Maxwellian plasma is given by Langmuir's orbital-motion theory as follows[1]:

$$\text{Sphere:} \quad I \cong eJ_r(1 + \eta_p), \tag{1}$$

$$\text{Cylinder:} \quad I \cong 2\pi^{-\frac{1}{2}}eJ_r(1 + \eta_p)^{\frac{1}{2}}, \tag{2}$$

where $\eta_p = -eV_p/kT_e$ is the normalized probe potential and J_r is the total random ion flux:

$$\text{Sphere:} \quad J_r = 4\pi r_p^2(kT_i/2\pi m_i)^{\frac{1}{2}}n_0, \tag{3}$$

$$\text{Cylinder:} \quad J_r = 2\pi r_p l(kT_i/2\pi m_i)^{\frac{1}{2}}n_0, \tag{4}$$

n_0 being the plasma density far from the probe. In the limit $\xi_p \gg 10$, the ion current is approximately the Bohm current[4]:

$$\text{Sphere:} \quad I_B \cong e\pi r_p^2(2kT_e/m_i)^{\frac{1}{2}}n_0\iota_B, \tag{5}$$

$$\text{Cylinder:} \quad I_B \cong 2er_p l(2kT_e/m_i)^{\frac{1}{2}}n_0\iota_B, \tag{6}$$

where ι_B is a weak function of T_i/T_e plotted by Chen.[4] For intermediate values of ξ_p, a theory approximating the ion distribution with a monoenergetic one has been given by Bernstein and Rabinowitz.[6] The numerical computations of the latter have been side-stepped by Lam,[7] whose boundary-layer analysis yielded a universal I–V curve. This curve is not very accurate, however, for ξ_p as low as 20; but a slightly more complicated modified Lam theory[3] is accurate to smaller values of ξ_p, as we shall show. The above theories for monoenergetic ions have been superseded by the recent work of Laframboise,[2] who has succeeded in devising a computer program for the case of a Maxwellian ion distribution and arbitrary ξ_p.

The results of Laframboise are presented in the form of cross plots between pairs of the quantities η_p, ξ_p, T_i/T_e, and $i_+ = J_i/J_r$. These graphs are easy to use and convey a great deal of physical insight. For instance, since the monoenergetic-ion and orbital-motion results are also given, one can see the ranges in which these approximations are good. In particular, one finds that the Maxwellian distribution smooths out the discontinuity in the i_+ versus ξ_p curve for a monoenergetic distribution due to the onset of orbital-motion limitation, but that the monoenergetic approximation is unlikely to be in error by more than 10%. To obtain the theoretical curves for Figs. 5 and 6, we assumed a value of n_0 and thus calculated λ_D and ξ_p. Then i_+ was obtained from a plot of i_+ versus ξ_p for $T_i = T_e$ and for various η_p. Using the same value of n_0,

[6] I. B. Bernstein and I. Rabinowitz, Phys. Fluids 2, 112 (1959).

[7] S. H. Lam, Phys. Fluids 8, 73 (1965).

we then obtained I_i from i_+. To obtain the theoretical curves for Figs. 7 and 8, we fixed η_p at 20 and computed I_i and n_0 for various ξ_p from Laframboise's graphs of i_+ versus η_p.

To obtain the net probe current $I = I_i - I_e$ shown on Figs. 5 and 6, one must subtract the electron component $I_e = eJ_{re}\exp(-\eta_p)$ from the ion component, where J_{re} is the random electron flux. Since η_p is referenced to the space potential V_s, this subtraction is sensitive to what one chooses for V_s. In a magnetic field the position of V_s on the I–V curve is not simply related to the knee on the curve where electron saturation sets in, as it is in the absence of a magnetic field. We therefore computed the floating potential $\eta_f = -e(V_f - V_s)/kT_e$ to find the position of V_s relative to the measured V_f. To do this, we took the projected area of the probe in computing J_{re}, since the electron Larmor radius is much smaller than r_p, and equated I_i to I_e. This resulted in the equations

$$\text{Sphere:} \qquad i_+ = \tfrac{1}{2}(m_i/m_e)^{\frac{1}{2}}e^{-\eta_f}, \tag{7}$$

$$\text{Cylinder:} \qquad i_+ = \frac{2}{\pi}(m_i/m_e)^{\frac{1}{2}}e^{-\eta_f}. \tag{8}$$

These curves were plotted on Laframboise's graphs of i_+ versus η_p, and the intersections with the curves of i_+ for various ξ_p gave η_f as a function of ξ_p. This turns out to be a weak function varying from 3.5–4.3 for spheres and from 4.1–4.6 for cylinders as ξ_p varies from 1 to 50 for $T_i = T_e$. An initial guess for n_0, and hence ξ_p, was sufficient to determine V_s relative to V_f.

Although Laframboise's results are definitive, they may not be generally available and may not cover the measured parameter range—for instance, the range $\eta_p > 25$. Consequently, we have also used the modified Lam theory.[3] This was necessary only for spherical probes, since our cylindrical probes operated in the region where the orbital-motion approximation, Eq. (2), agreed with the exact result of Laframboise. Lam's theory requires the simultaneous solution of the equations

$$\frac{-V_p}{I_i^{\frac{2}{3}}} = \left(\frac{m_i}{2e}\right)^{\frac{1}{3}} F\left[\left(\frac{j}{j_m}\right)^{\frac{1}{2}}\right] \tag{9}$$

and

$$j_m = j_B\left[1 + 3.45\left(\frac{j_m}{j}\right)^{2/5}\xi_p^{-4/5}\right]^2, \tag{10}$$

where F is a universal function of its argument and

$$I_i = e\pi r_p^2 n_0[2(1+\beta)kT_e/m_i]^{\frac{1}{2}}, \tag{11}$$

β being $4/\pi$ for $T_i = T_e$. If we define $\tau \equiv j/j_m$, $F(\tau^{\frac{1}{2}}) \equiv \Lambda_s(\tau)$, and $\iota_B = j_B(1+\beta)^{\frac{1}{2}}$, a little manipulation brings Eq. (9) into the form

$$Y \equiv \left(\frac{j_m}{j_B}\right)^{\frac{2}{3}} = \frac{\eta_p}{\tau^{\frac{2}{3}}\Lambda_s(\tau)}\left(\frac{4}{\iota_B}\frac{1}{\xi_p^2}\right)^{\frac{1}{3}}. \tag{12}$$

Similarly, Eq. (10) can be written

$$Y \equiv \left(\frac{j_m}{j_B}\right)^{2/3} = [1 + 3.45\tau^{-2/5}\xi_p^{-4/5}]^{4/3}. \tag{13}$$

The functions $\tau^{\frac{2}{3}}\Lambda_s(\tau)$ and $\iota_B(\beta)$ are given by Chen.[4]

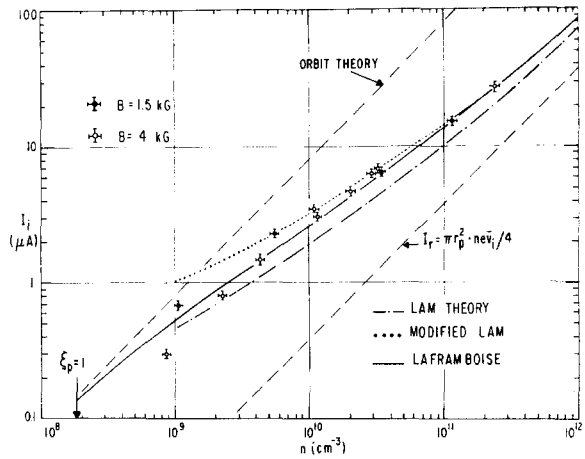

FIG. 7. Measured values of I_i for a spherical probe at $\eta_p = 20$, as a function of plasma density as determined by microwaves, for two values of magnetic field. The theoretical curves are explained in the text. In this range of ξ_p, neither the random ion current I_r nor the orbital-motion-limited current (dashed lines) is a good approximation. Probe radius: 0.025 cm.

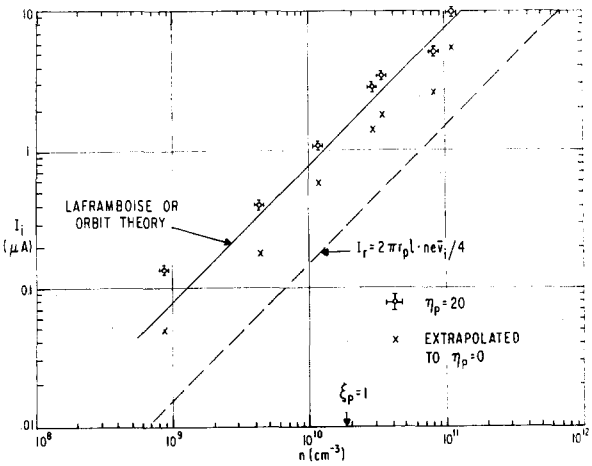

FIG. 8. Measured values of I_i for a cylindrical probe at $\eta_p = 20$ (circles), as a function of plasma density as determined by microwaves, for $B = 4$ kG. The solid theoretical curve is from the exact computations of Laframboise, which is essentially identical with the orbital-motion approximation in this range of ξ_p. The values of I_i at $\eta_p = 0$ (crosses), obtained by extrapolation, are to be compared with the dashed line representing the random ion current. Probe radius: 0.0028 cm. Probe length: 0.19 cm.

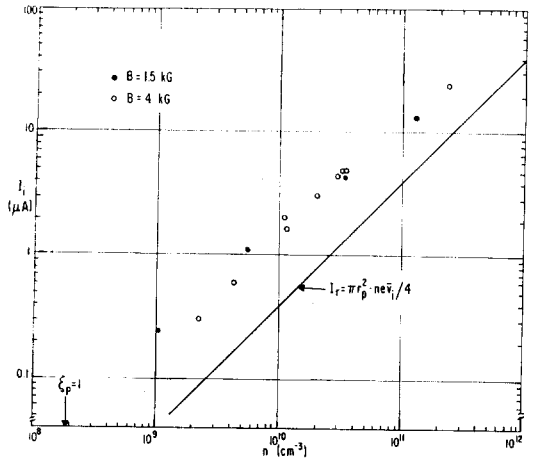

FIG. 9. Measured values of I_i at $\eta_p = 0$, obtained by extrapolating the same I–V curves used for Fig. 7, as a function of microwave-determined density. The solid line shows the random ion current.

For each choice of a pair (η_p, n_0), Eqs. (12) and (13) gave two curves of Y versus τ whose intersection gave the values of Y and τ for the given values of η_p and n_0. The probe current was then found from

$$I_i = I_B(Y\tau^{\frac{3}{2}})^{\frac{3}{5}}, \tag{14}$$

with I_B given by Eq. (5). The lowest-order theory of Lam[7] is recovered by replacing Eq. (13) with $Y = 1$. It was in this manner that the Lam curves of Figs. 5 and 7 were computed.

E. Measurements of I_i

Figures 5 and 6 show typical I–V curves for spherical and cylindrical probes, respectively. The experimental points were taken directly from the original x-y recorder traces. The theoretical curves were computed as described above. We assumed $T_i = T_e = T_c = 2580°\text{K}$ throughout. Note that the shape of the curves agrees well with theory out to $\eta_p = 400$. The deviation at very large η_p in the spherical case is probably due to the limitations of the modified Lam theory.

In Figs. 7 and 8 we show the probe current at $\eta_p = 20$ versus density as measured by microwaves, as described below. The spherical and cylindrical probe data were taken at the same point in the plasma by alternately removing each probe. Two cylindrical-probe points that fell far below the curve have been omitted; the probe was obviously contaminated. The value of I_i was read off saturation current curves such as those shown in Figs. 5 and 6 by using the computed position of V_s and $kT_e = 0.222$ eV to find the $\eta_p = 20$ point. In the case of the spherical probe, a correction was made for the current collected by the unshielded support wire. This correction could have been made by subtracting a proportionate fraction of the current to a cylindrical probe at the same point; however, the measured cylindrical-probe current includes end-collection, and what we have subtracted is the theoretical cylindrical-probe current at the measured density.

In Figs. 9 and 8, respectively, we also show the ion current to spherical and cylindrical probes at $\eta_p = 0$, obtained by straight-line extrapolation of the I–V curve to the calculated value of V_s, as shown by the dashed lines in Figs. 5 and 6. If this current is equated to the random ion current, as is frequently done,[8] a large error results. In Fig. 9 no correction was made for the current to the support wire.

F. Errors

This experiment was designed for 10% accuracy, and no pains were taken to eliminate sources of error smaller than this order of magnitude. The largest uncertainty is in the probe area. In the cylindrical case, the jaggedness of the end of the glass insulator made l hard to measure. It is possible that ions "leaked" past the end of the insulator. End-collection was not corrected for. These effects are in a direction to reduce the discrepancy between theory and experiment but are probably less than 10%. In the spherical case, a correction of 10–20% was made for the support wire; the error in the correction was therefore probably less than 10%. No correction was made for the wire hook below the sphere (Fig. 2). This could account for the small discrepancy between theory and experiment, but we do not know how to correct for this. Nonsphericity of the probe was less than 10%. Partial contamination of the probe surface would have shown up as a scatter in the data, which were taken in different runs over a period of three weeks, with the vacuum opened in between. Errors in the assumed values of T_i and T_e could possibly lead to an error of 10% in n_0. Deviations from Maxwellian distributions and an error in the computed value of V_s would lead to errors $\ll 10\%$. The effect of the magnetic field for our ratio of r_p to r_L is seen from Fig. 7 to be greater than 10%. This is not an error; it is an effect we wished to measure.

The amplitude of low-frequency oscillations n_1/n_0 ranged from 0.15–0.01 as n_0 and B were varied.

[8] M. Hashmi, A. J. van der Houven van Oordt, and J. G. Wegrowe, in *Proceedings of the Conference on Physics of Quiescent Plasmas* (Laboratori Gas Ionizzati, Frascati, Italy, 1967), Pt. II, p. 523.

Since the microwave cavity frequency shift is proportional to n_0 but the probe current is not quite proportional to n_0 in our range of ξ_p, the probe and microwave measurements take a different average over the fluctuations. This effect is estimated to be less than 10%.

On the theoretical side, the Laframboise curves are good to 0.2%, but the modified Lam theory can be expected to be in error by much more than 10% for $\xi_p = O(1)$. Both theories give limits on r_p and η_p beyond which ions can be trapped in closed orbits around the probe. The experiment lies well inside the range of possible ion trapping, but the agreement between theory and experiment for all values of η_p (Figs. 5 and 6) shows that trapping is not important. The discrepancy at large η_p in Fig. 5 is in the opposite direction from what would be expected if ion trapping occurred.

III. MICROWAVE CAVITY

The aluminum cavity shown in Fig. 1 has an internal radius a of 6.825 cm and a free-air resonance frequency $\omega_r/2\pi$ of 1736.1 ± 0.1 MHz for the TM_{010} mode. The short cylinders of approximately half this radius at the ends of the cavity are waveguides beyond cutoff for the resonance frequency and allow a Q of about 10^3 to be achieved in the absence of plasma in spite of the relatively large holes in the end plates of the cavity. Except for the fringing fields caused by these holes, the electric field in the TM_{010} mode is parallel to the axis, and the magnetic field should have no effect on the resonance frequency. This type of cavity was first tested by Lustig.[9] Coupling of microwave power from the swept-frequency generator to the cavity was partly electrostatic and partly electromagnetic. The reflected power from the cavity was rectified and displayed on an oscilloscope along with the resonance peak from a frequency meter.

The frequency shift $\Delta\omega/\omega_r$ caused by the presence of plasma is found by perturbation analysis for the TM_{010} mode to be[10]

$$\frac{\Delta\omega}{\omega_r} = \frac{1}{2}\left(\frac{\omega_{p0}}{\omega_r}\right)^2 \int_0^R \frac{n(r)}{n_p} \cdot J_0^2\left(\frac{2.4r}{a}\right) r\,dr \Big/ \int_0^a J_0^2\left(\frac{2.4r}{a}\right) r\,dr, \qquad (15)$$

where R is the plasma radius, $n(r)$ the density profile, n_p the peak density, and ω_{p0} the plasma frequency at the peak. The peak density, and hence the density at the position of the probe, was found by integrating Eq. (15) numerically over the measured density profile. Such a profile is shown in Fig. 10. Scans were also made in other azimuthal directions. It was found that neither the azimuthal asymmetry nor the variation of the profile from run to run affected the integration by more than 10%. However, when the magnetic field was varied, the profile changed enough to require a separate integration.

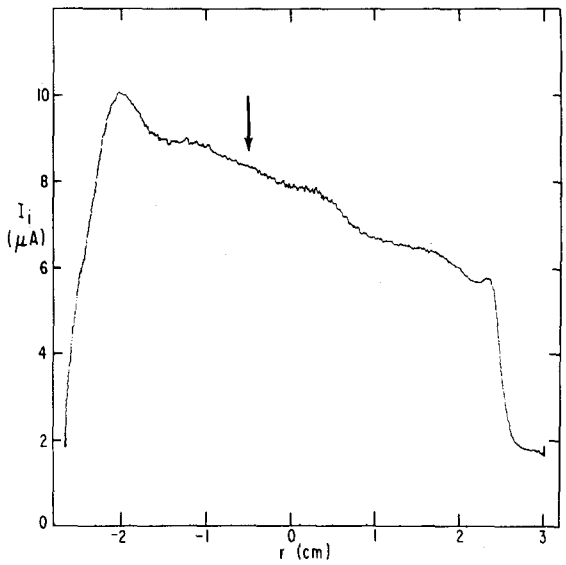

FIG. 10. Typical density profile, as indicated by the saturation ion current, at 4 kG. The arrow indicates the relatively flat region where the probe data were taken. The density nonuniformity was caused by a small temperature gradient across one or both end plates but did not affect the accuracy of this experiment since it was taken into account.

It is well known from the work of Buchsbaum, Mower, and Brown[10] and of Agdur and Enander[11] that the perturbation analysis is valid up to values of ω_p well above ω_r. However, our ratio of $a/R = 2.5$ was lower than in their computations, and we had to repeat these computations using Eq. (2.4) of Ref. 10 for the exact solution. Figure 11 shows the resulting comparison between the exact and perturbation analyses for $a/R = 2.5$ and uniform plasma density. It is seen that the perturbation analysis is accurate to 10% for densities up to 2.5 times the critical density $n_c = 3.7 \times 10^{10}$ cm^{-3} where $\omega_p = \omega_r$. In practice the cavity measurement was limited to $n \leq n_c$ because the resonance peak became so broad that it was hard to distinguish from other low-Q resonances. We have also tried

[9] C. D. Lustig, Project Matterhorn Microwave Memo No. 7 (1960).

[10] S. J. Buchsbaum, L. Mower, and S. C. Brown, Phys. Fluids **3**, 806 (1960).

[11] B. Agdur and B. Enander, J. Appl. Phys. **33**, 575 (1962).

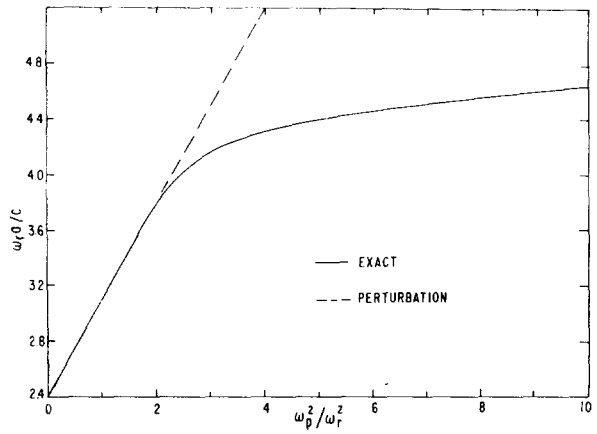

FIG. 11. The resonance frequency of a TM_{010} cavity with $a/R = 2.5$, as given by the exact and perturbation analyses for a uniform plasma.

using the entire vacuum chamber as a cavity, but the $k_\parallel \neq 0$ modes are so numerous in such a long cavity that the TM_{010} resonance was not identifiable.

To account for the fringing fields caused by the large holes in the cavity, we calibrated the cavity with a long rod of polystyrene foam with the same diameter and the same order of magnitude of $\epsilon - 1$ as the plasma (but of opposite sign), ϵ being the dielectric constant. Since the value of ϵ obtained by weighing the rod gave obviously erroneous results, it was necessary to measure ϵ as follows. The cavity was made into an ideal cavity by filling the waveguide sections of the cavity with aluminum plugs, which were flush with the end walls of the cavity. The resonance frequency of this ideal cavity, without fringing fields, was then measured with and without a polyfoam rod. In this manner, it was found that Eq. (15) gave a frequency shift that was 9% too low; consequently, the plasma density deduced from Eq. (15) and the measured $\Delta\omega$ was increased by 9%. The error in this correction was probably well within the 10% accuracy of the experiment.

Unfortunately, the effect of the magnetic field could not be determined this way and had to be estimated theoretically. To do this, we assumed that a fraction α of the total frequency shift was due to a TE_{011} mode in the waveguide sections of the cavity. Using Eq. (4.4) of Ref. 10, we computed the effect of B on the frequency shift due to this mode. This turned out to be 21% at 1.5 kG and 2.5% at 4 kG. The work of Lustig[9] indicated that about 27% of the total frequency shift came from the waveguide sections. If we now make the very pessimistic assumption that all of this 27% is due to the TE_{011} mode, which is sensitive to B, so that $\alpha = 0.27$, we would find that the total $\Delta\omega$ is decreased by 5.6% at 1.5 kG and 0.7% at 4 kG. Both of these figures are within the 10% experimental accuracy.

IV. MICROWAVE INTERFEROMETRY

To measure densities above 3×10^{10} cm^{-3}, we used an 8-mm microwave interferometer designed by Ernst[12] for use with steady-state plasmas. The 35-GHz signal sent through the plasma leg of the interferometer is first modulated by a 30-MHz single-sideband modulator. The transmitted signal is then mixed with the unmodulated signal from the dummy leg, amplified by a 30-MHz-i.f. amplifier, and further heterodyned down to 100 kHz, along with an un-phase-shifted signal from the modulator. The phase shift between the two 100 kHz signals, which is the same as the phase shift introduced by the plasma, could then be read directly from a phase meter. The density was computed from the standard formula[13] for a plane plasma slab, with integration over the measured density profile between the microwave horns.

In pulsed plasmas it is possible,[14] by carefully matching the lengths of the plasma leg and the dummy leg, to measure down to $n = 10^9$ cm^{-3} by 8-mm interferometry. Our plasma, however, could be turned off only by cooling the hot end plates or by dropping collectors in at the two ends of the machine. Either of these procedures required many seconds, during which thermal drifts made phase shift measurements of the order of 1° impossible. It did not help to switch between the plasma leg and a dummy leg containing a variable phase shifter and attenuator to approximate the zero-plasma conditions, for this caused mechanical vibration of the waveguides. Without undue expenditure of time, we could not measure with sufficient accuracy phase shifts below 7°, and hence densities below $\sim 10^{11}$ cm^{-3}. Only the last two points in Figs. 7–9 were obtained by this technique.

V. PROPAGATION OF ELECTRON PLASMA WAVES

A. Introduction

For $\omega < \omega_p$, electron plasma waves can propagate freely along a plasma column in a strong magnetic field ($\omega_p \ll \omega_{ce}$); in the neighborhood of ω_p, however, the group velocity of these waves decreases sharply,

[12] W. P. Ernst, ISA Trans. 3, No. 1, 53.2.62-1 (1964).
[13] M. A. Heald and C. B. Wharton, *Plasma Diagnostics with Microwaves* (John Wiley & Sons, New York, 1965), p. 214.
[14] W. Stodiek, D. J. Grove, G. Hsi, E. B. Meservey, and M. G. Rusbridge, Princeton Plasma Physics Laboratory MATT-Q-24 (1966), p. 1.

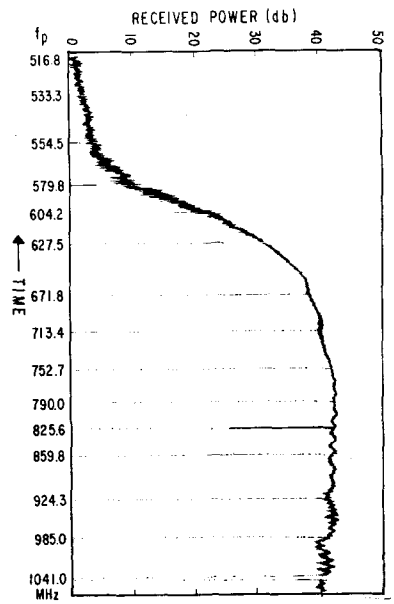

FIG. 12. An x-y recorder trace of the power at 700 MHz transmitted between two probes as a function of time. The plasma frequency of the decaying plasma, as measured by the microwave cavity, is shown at the marker points on the abscissa. On the left we have $\omega > \omega_p$, and on the right, $\omega < \omega_p$.

and the Landau and collisional damping mechanisms become important. The sharp variation in absorption near $\omega = \omega_p$ has been proposed[15] as a method for measuring plasma density.

B. Measurements

The two shielded spherical probes (Fig. 1) are aligned along the magnetic field 30 cm apart at the density maximum (Fig. 10). The waves are launched by connecting one probe to a 200–300 mW oscillator and received by connecting the other probe to a government surplus receiver tuned to the transmitted frequency. The i.f. output of the receiver is then connected to a logarithmic converter driving the y axis of an x-y recorder. The x axis is swept in time as the plasma density is decreased by allowing the neutral-beam ovens to cool. During this slow decay, the plasma density is measured periodically by the microwave cavity method at times marked on the recorder trace. An example of such a trace is shown in Fig. 12. A change of 40 dB in received power is observed in the vicinity of $\omega = \omega_p$.

During the cooling of the ovens, the ion fluxes from the two ends of the machine are not necessarily balanced, so that a macroscopic drift of the plasma can occur. Although probes would be affected by this drift, neither the cavity nor the propagation method is sensitive to it. Instead of working at fixed ω, we have also varied ω at fixed density, but corrections for the variations in the oscillator output are tedious.

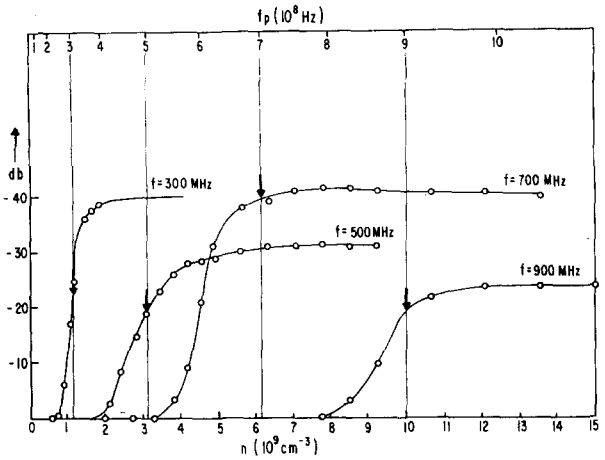

FIG. 13. Results of propagation measurements at 300, 500, 700, and 900 MHz. Received power is plotted against plasma density and plasma frequency as measured by the cavity method. The errors indicate the points $\omega = \omega_p$.

In Fig. 13 we show measurements of received power versus peak density at four frequencies. A cutoff always occurs in the vicinity of $\omega = \omega_p$, and the width of the cutoff is about 20–40% on the density scale.

C. Theory

The potential ϕ in an electron plasma wave in a strong magnetic field satisfies the wave equation

$$\left(\frac{\partial^2}{\partial r^2} + \frac{1}{r}\frac{\partial}{\partial r} - \frac{m^2}{r^2}\right)\phi - \epsilon_{zz}k_\parallel^2\phi = 0, \qquad (16)$$

where m is the azimuthal mode number. The element ϵ_{zz} of the dielectric tensor is given for a collisionless plasma by

$$\epsilon_{zz} = 1 - (\omega_p^2/\omega^2)\zeta^2 Z'(\zeta), \qquad (17)$$

where $\zeta \equiv \omega/k_\parallel v_{th}$ and $Z(\zeta)$ is the plasma dispersion function.[16] If we write $k_\parallel = k_r + ik_i$ with $|k_i| \ll |k_r|$, we have $\zeta = x + iy$, with $x = \omega/k_r v_{th}$, $y = -xk_i/k_r$. We wish first to evaluate the absorption in the vicinity of $\omega = \omega_p$. This can be done in a simple way by considering a homogeneous plasma filling a cylindrical waveguide of radius a. The dispersion relation then reads

$$\epsilon_{zz}k_\parallel^2 + a^{-2}p_{mn}^2 = 0, \qquad (18)$$

where p_{mn} is the nth root of the mth Bessel function

[15] R. Cano, C. Etievant, I. Fidone, M. Mattioli, J. Olivain, and M. Perulli, Compt. Rend. **263B**, 439 (1966).

[16] B. D. Fried and S. D. Conte, *The Plasma Dispersion Function* (Academic Press Inc., New York, 1961).

J_m. Equations (17) and (18) give

$$Z'(\zeta) = \left(\frac{\omega^2}{\omega_p^2}\frac{p_{mn}^2}{a^2}\frac{v_{\text{th}}^2}{\omega^2} + \frac{1}{\zeta^2}\right). \tag{19}$$

Separating the real and imaginary parts, we obtain

$$\frac{\omega^2}{\omega_p^2} = \text{Re } Z'(x)\left[\frac{p_{mn}^2}{a^2}\frac{v_{\text{th}}^2}{\omega^2} + \frac{1}{x^2}\right]^{-1}, \tag{20}$$

$$2\left(\frac{\omega^2}{\omega_p^2}\right)\frac{y}{x^3} = -\text{Im } Z'(x). \tag{21}$$

For $x \gg 1$, Eqs. (20) and (21) may be approximated by

$$\frac{\omega^2}{\omega_p^2} = \frac{1 + (3/2x^2)}{1 + (p_{mn}^2 v_{\text{th}}^2/a^2\omega^2)}, \tag{22}$$

$$\frac{y}{x} = \frac{\frac{1}{2}\Gamma}{1 - (\omega_p^2/\omega^2)(1 + 3/x^2)}. \tag{23}$$

For Landau damping, we have

$$\Gamma = \Gamma_L = 2\pi^{\frac{1}{2}}(\omega_p^2/\omega^2)x^3 e^{-x^2}. \tag{24}$$

Equations (22) and (23) are valid also for the case of collisional damping with $\nu_e \gg \omega$ if we use the following expression[17] for Γ:

$$\Gamma = \Gamma_{\text{coll}} = \frac{\omega_p^2}{\omega^2}\frac{\nu_e}{\omega}\left(1 + \frac{3}{2x^2} + \cdots\right). \tag{25}$$

When the neutral pressure is sufficiently low, as in our experiment, only electron–ion collisions are important, and we may use in Eq. (25) the collision frequency for 90° deflection given by Spitzer.[18]

D. Discussion of Results

Using Eqs. (20) to (25), we have estimated the damping for the least damped mode ($p_{mn} = p_{01} = 2.4$) in our experiment. We find that in all cases Landau damping abruptly cuts off the transmission in the region $1.1 < \omega^2/\omega_p^2 < 1.2$. For the two high-density cases, collisional damping is more important than Landau damping and occurs in the range $0.9 < \omega^2/\omega_p^2 < 1.1$. For $\omega^2/\omega_p^2 < 0.9$, the wave propagates with less than 5-dB attenuation over the 30-cm distance between probes. At $\omega = \omega_p$, the collisional absorption is 12 dB at 300 MHz, 25 dB at 500 MHz, 62 dB at 700 MHz, and 115 dB at 900 MHz.

The observed cutoff in transmission can therefore be considered as the result of a combination of collisional and Landau damping. Collisions start the cutoff in the range $0.9 < \omega^2/\omega_p^2 < 1.1$, and Landau damping completes the cutoff for $\omega^2/\omega_p^2 > 1.1$. In the 700 and 900 MHz cases, collisional damping is dominant and absorption sets in for $\omega < \omega_p$; in the 300 and 500 MHz cases, Landau damping is dominant, and absorption sets in for $\omega \approx 1.07\omega_p$. However, the computed width $\Delta\omega/\omega$ of the cutoff varies from 5% at 900 MHz to 10% at 300 MHz, about a factor of 2 less than observed. We believe the discrepancy is caused by the density fluctuations in the plasma, which allow transmission during part of each cycle even when $\omega > 1.07\langle\omega_p\rangle$. The magnitude of the fluctuations (Sec. IIF) is entirely consistent with this interpretation. If the theoretical cutoff were infinitely sharp and the observed width were due entirely to oscillations, the average density would be given by the 3-dB points on the curves of Fig. 13. A further effect arises from the inhomogeneity of the plasma and the existence of higher modes p_{mn}. Both these effects tend to increase $k_\perp$ and make the damping start at a higher value of density. Finally, the coupling of power through the sheaths on the probes may vary with density.

In conclusion, the measurements described here show that the plasma density is measured to within 20% if the point at which the transmitted signal drops by 3 dB is simply identified with the condition $\omega = \omega_p$. The broadening of the cutoff caused by oscillations precluded a more accurate treatment including the variation of the absorption point with density and the more subtle points listed above. The main advantage of this method is its simplicity; a modicum of equipment and forethought is required, and the results are insensitive to probe contamination. A limitation of the method is that only low densities such that $\omega_p < \omega_{c0}$ can be measured, where ω_{c0} is the waveguide cutoff of the vacuum chamber. Otherwise, propagation can occur through electromagnetic modes. If the chamber contains an internal conductor, such as a "hard-core," it becomes a transmission line; and propagation occurs at all frequencies. The method is also limited to $\omega_p < \omega_{ce}$; otherwise coupling occurs through cyclotron modes. Note that only the peak density is measured, because waves traveling along the density maximum are the last to disappear.

VI. SUMMARY

The results shown in Fig. 7 indicate that Langmuir probes can measure the plasma density to within 10% down to $\xi_p \approx 10$ and to within ~25% down to $\xi_p \approx 2$ if Laframboise's[2] computations are used.

[17] W. P. Allis, S. J. Buchsbaum, and A. Bers, *Waves in Anisotropic Plasmas* (M.I.T. Press, Cambridge, Massachusetts, 1963), p. 90.

[18] L. Spitzer, Jr., *Physics of Fully Ionized Gases* (John Wiley & Sons, New York, 1962), 2nd ed., Eq. (5–22).

Lam's[7] lowest-order theory is in error by 50% in some ranges, but the modified Lam theory[3] is surprisingly accurate down to $\xi_p \approx 5$. The effect of the magnetic field can be seen at low densities, where the collection radius r_s becomes comparable to r_L, causing the 4-kG points to lie below the 1.5-kG points. The fact that at higher densities there is agreement between the 4-kG and 1.5-kG data means that our ratio of $r_p/r_L = 0.25$ is small enough. One cannot avoid the effects of B at low densities when λ_D/r_L becomes appreciable. If the 1.5-kG points can be considered to be unaffected by B, then it would appear that the probe currents at low density are higher than predicted, by an amount slightly outside the experimental error.

The data of Fig. 7 span the range of ξ_p between the low range, where the orbital-motion approximation is valid, and the high range, where the Bohm formula, Eq. (5), is valid. In the limit of large or small ξ_p, n is proportional to I_i, but it is seen from Fig. 7 that in the transition region n varies more nearly as $I_i^{\frac{1}{2}}$. This will affect measurements of density profile in low-density plasmas.

In Fig. 9, it is seen that equating the extrapolated ion current to the random ion current can lead to an error of a factor of 6. For cylindrical probes, this procedure leads to an error of a factor of 4, as seen from Fig. 8.

Figure 8 shows that a cylindrical probe can be made to operate in the region of orbital-motion-limited current, where n is proportional to I_i. Unfortunately, the measured probe currents are systematically about 30% higher than predicted. Part of this discrepancy is due to end-collection by the probe; the rest is unexplained.

To improve the accuracy of the present experiment, one would have to measure the collecting area of the probe more precisely, to calibrate the microwave cavity more accurately for the effects of magnetic field and fringing electric field, and to integrate over the plasma profile more carefully in reducing the microwave data.

For probe measurements in low-density plasmas we arrive at the following recommendations. If the requirements of spatial and temporal resolution permit, one should use a cylindrical probe with $r_p \ll r_L \ll l$ and $\xi_p \lesssim O(1)$. The orbital-motion-limited current approximation can then be used. If r_p and kT are approximately the same as in this experiment, Fig. 8 can be used as a calibration curve if scaled properly for the differences in r_p, l, and kT. If $\xi_p > O(1)$ must be used, one should use a spherical probe, interpreted according to the Laframboise[2] or Lam[3] theory. Once r_p and η_p are chosen, a theoretical curve of I_i versus n can be drawn up, as in Fig. 8, to be used during the experiment. The use of short cylindrical probes with $\xi_p \gtrsim O(1)$ can lead to accurate results only by accident.

Finally, we wish to point out that although this paper covers only dc measurements, the problem of measuring fluctuations in a low-density plasma is a severe one, particularly if fluctuations in potential are involved. This problem has been discussed in a separate paper.[19]

ACKNOWLEDGMENTS

Design and construction of the microwave cavity and of the microwave interferometer were carried out by W. Ernst and A. Skislak, whose help was indispensable. The probes were fabricated by W. Lamont, and the L-2Q machine was operated by K. P. Mann, to both of whom we are grateful. R. Chang assisted in the reduction of the microwave data.

This work was performed under the auspices of the United States Atomic Energy Commission, Contract No. AT(30-1)-1238.

[19] F. F. Chen, in *Proceedings of the Conference on Physics of Quiescent Plasmas* (Laboratori Gas Ionizzati, Frascati, Italy, 1967), Pt. II, p. 563.